Surface and Air Picture Compilation with Multiple Naval Radar Systems

Umesh Ramdaras[*] & Frans Absil

Introduction

Recent advances in Information and Communication Technology have had their effect on the architecture and the concept of operations for military systems. Increased connectivity of sensor, weapon and command and control (C2) systems is an enabler for *Network Centric Warfare* (NCW) [Alberts et al., 2000], [Cebrowski and Garstka, 1998]. The NCW concept, essentially a *distributed system*, may be depicted as a layered set of three grids: a sensor, shooter (i.e., weapons) and information grid, with the grid nodes representing individual military systems. The links within and between the grids represent the connectivity.

Introducing such a concept will have an effect on military operations; this effect is denoted as Network-Enabled Capabilities (NEC). Key NEC characteristics and processes are:

- multi-sensor data fusion, i.e., using observations from a multitude of sensor systems to compile an integrated operational picture;
- increased situational awareness, i.e., a better understanding of the operational picture in terms of military threats and own capabilities;
- information superiority. Through increased connectivity and higher link bandwidths (enabling higher data transfer rates) all parties in the network should have faster and better knowledge of the current battlefield status than an opponent who has no or a less capable network.
- A more rapid C2 loop, also indicated as the Object-Orient-Decide-Act loop [Boyd, 1992]. Based on the previous processes and with increased connectivity between Command, Control and Communication (C3) systems, the commander should be able to increase the pace of decision making and keep the momentum on the battlefield. This includes quick assessment of the outcome of the military effect.
- Modernisation of the command hierarchy, indicated by terms such as self-synchronisation and delegated authority (see [Alberts et al., 2000]).

These developments will obviously affect maritime operations. Typical surface ships such as corvettes, frigates and cruisers may contain a suite of sensor systems, dedicated to a specific warfare domain. Radar systems will search, detect and track air and surface objects, while sonars are listening for underwater sources. Typically, electro-optic systems (video, infrared, night vision, etc.) are used near the sea-air interface. Sensor systems may also play a role in the fire control process, when deploying weapon systems. The role of the combat system designer is to integrate the on-board sensor, weapon and C3 systems (the hardware) and implement military capability in the system architecture through a Combat Management System (CMS, i.e., the software).

[*] Umesh Ramdaras is with the Combat Systems Department of the Netherlands Defence Academy as well as with the International Research Centre for Telecommunications and Radar of the Delft University of Technology.

Coordinated system deployment is already an issue on a single ship. Modern, electronically steered radar systems, such as the Thales SMART-L and the APAR on-board of the RNLN Air Defence and Command Frigate have the capability to rapidly switch between radar modes or functions, and to adapt the radar settings for each of the modes or functions. Maximising the benefit from such advanced radar systems requires optimisation of their deployment and settings, a process known as *sensor management*. Also coordination between ship, sensor and communication systems is required, e.g., to prevent interference for systems with overlapping operational frequency ranges.

Moving towards an NCW architecture the coordination between multiple ships, or between ships and other platforms, such as combat aircraft, helicopters or Unmanned Aerial Vehicles (UAVs), will require attention. In a distributed system the optimisation process is extended over multiple platforms, each potentially equipped with multiple sensors. Obviously, the degree of complexity increases. Limited coordination between multiple platforms already has been achieved with communication and data link systems (e.g., Link-16, Link-22), where various data types (message, voice, video, etc.) at the tactical or strategic level are shared between units. Also, the concept of Cooperative Engagement Capability, distributing raw radar data between ships, has been tested at sea [Johns Hopkins APL, 1995], [Sijtsma, 1995].

In order to realise the capability of a NCW systems concept the coordination between various naval units will have to be increased. The CMS may have to extend its functionality over multiple platforms, and sensor management will have to be applied across ships. The Netherlands Defence Academy (NLDA) has taken up this topic in a research program.

Automatic sensor management was investigated in a collaborative research initiative, called the STATOR (Sensor Timing And Tuning on Object Request, 2003-2005) project [STATOR, 2005]. This paper gives an overview of a second PhD thesis research project, started in 2004 as a contribution to the previous activities; sensor coordination is extended to a group of moving platforms. A network of maritime radar systems used for air and surface picture compilation will be considered. Sensor management may be divided into *sensor selection* and *sensor localisation*. The outcome of the sensor selection process is the appropriate sensor for doing an observation, while sensor localisation will position the platforms such, that they can best deploy their sensor capabilities in the near future. Terminology like 'appropriate' and 'best deployment' imply an *optimisation process*, minimising a *cost function* that acts as the driver mechanism for sensor selection and localisation.

With a properly working sensor selection process, global sensor deployment (for the entire sensor suite in the network) can be optimised. Suppose that for a given target scenario one is able to identify the best sensor to observe that target within a certain planning horizon, i.e., a number of time intervals ahead; in the meantime the other sensors might be used for other tasks, reducing overlapping observations and redundant sensor measurements. Current practice in maritime operations is space (e.g., allocating search areas or sectors to specific ships in a task group) and time domain separation in

the planning stage of an operation. An adaptive and near real time sensor allocation mechanism would mean a significant step forward towards implementing NEC, and would make better use of the distributed sensor resources.

This work will be limited to the task of *target tracking*, as part of the operational picture compilation process. Target tracking means that a sequence of sensor observations will be used (not necessarily from the same sensor) to estimate the target *state vector*, i.e., a set of attributes characterising the target. These attributes may include target position, speed and course (heading), and manoeuvres (accelerations). The target state is time-dependent and therefore during the tracking process the state vector will be continuously updated.

The cost function, i.e., the decision metric for sensor management, is derived from the target state vector. It is a measure of the accuracy in the target state estimate and will contain certain elements from the *state error covariance matrix*. Which elements will be considered in the cost function may depend on the sensor task, or the stage of a military operation. For a long range surveillance task (e.g., in the range 100 – 200 km) one is not interested in a highly accurate estimate of target speed; neither is the target altitude highly relevant, so the elevation angle need not be estimated with high precision. A sufficiently accurate range and bearing angle will do. If the target is incoming (which by itself is the outcome of the estimation of the radial velocity component between target object and sensor; an approaching target implies a positive closing speed) a more accurate position, speed and heading estimate will become relevant. If at some point the target turns out to be a threat, the exact position in 3-dimensional space must be known at each time instant. Before deploying countermeasures one has to make sure that the target is within the operational envelope of defensive weapons. A guided weapon will need a good estimate of the relative geometry between target and intercepting missile; a gun fired will require a highly accurate estimate of the predicted hitting point of the projectiles (extremely high target position, speed and heading accuracy). In general, the cost function should be a variable, mission-related driver of the sensor selection process.

Sensors obviously have different performance characteristics. Radars may or may not determine the relative target radial velocity component through the Doppler shift measurement. The measurement accuracy might be different for elevation and azimuth angle. One sensor might outperform another in measuring a specific target characteristic. A sensor need not yield an observation, every time it is pointed (looking) at the target; in practice the detection probability is smaller than one and there will be missed detections. The varying sensor performance characteristics have to be incorporated into the sensor management process.

Selecting a sensor from the sensor grid to perform a task could be done in different ways. It might be carried out randomly or with a preference for a certain sensor. In both cases a sensor is selected without taking its suitability into account. On the other hand, sensor selection could be based on prior knowledge or actual performance. In the first case the knowledge, gained from experience in similar situations in the past or from experts, is translated into knowledge networks (e.g., Bayesian Networks [Yilmazer and Osadciw, 2004], Fuzzy Logic [Molina López et al., 1995], etc.). In the second case sensor selection is

based on the instantaneous performance measures of the sensors (e.g., the error covariance matrix).

The performance-based sensor selection algorithm (SSA), presented in [Ramdaras and Absil, 2006], compares sensors with respect to the *best expected performance*. For a specific scenario, at each time step within a planning horizon, the sensor with the relevant best expected target attribute accuracy does the observation. E.g., for a good target position estimate sensor selection will be determined by comparing the positional variance. Sensor performance evaluation is based on the Modified Riccati Equation (MRE). In [Boers and Driessen, 2006a, 2006b] it is shown that the best achievable error performance of the optimal state estimation filter, the Cramér-Rao Lower Bound (CRLB), has an upper bound determined by the solution of the MRE for the class of systems with probability of detection smaller than one. Besides, using the MRE yields a reduced computational load, compared to the CRLB.

In order to investigate the benefits of this MRE SSA, it has been compared to a selection algorithm based on the *trace* (diagonal elements) of the *updated predicted error covariance matrix* (TRACE SSA) [Chhetri et al., 2003]. In [Ramdaras and Absil, 2007a] results of the comparison of the MRE SSA with a random sensor selection (RSS) and a fixed sensor selection (FSS) scheme are included, while [Ramdaras and Absil, 2007b] presents simulation results for a set of different performance-based selection criteria. In all of these the effect of reduced detection probability of detection was taken into account.

However, remember that sensor selection may also be bounded by external factors that have to be taken into account. During a military operation rules of engagement will be in effect (e.g., prohibiting transmissions in certain bearing sectors). There may be criteria of physical nature (e.g., radar horizon, weather conditions) that limit the selection procedure.

This paper will give an overview of the sensor selection research topic. Results from an extensive MATLAB® computer simulation approach will be presented, assuming a single, non-moving platform with multiple sensors (the extension to multiple platforms is discussed at the end of the paper) and a single combat aircraft target. MRE based sensor selection strategies for different sensor selection criteria will be considered. Comparison between the MRE SSA and RSS, FSS and TRACE SSA will demonstrate the usability and benefits of the MRE SSA. Sensor selection strategies and performance evaluation will be discussed for several planning horizons and for various values of the detection probability.

State estimation

State estimation can be done with the Kalman Filter (KF) [Kalman, 1960], [Bar-Shalom and Fortmann, 1988], a first order recursive algorithm that will yield the minimum mean squared state estimate error for a linear state transition and observation model and assuming zero-mean Gaussian state vector and noise terms. The KF is used in many radar tracking applications as target state estimator.

Although extensions to the KF exist, the Particle Filter (PF) [Gordon et al., 1993] has become a popular method for stochastic dynamic estimation problems. This is due to the fact that it is possible to design for any nonlinear and non-Gaussian dynamic estimation problem an accurate, reliable and fast recursive Bayesian filter [Ristic et al., 2004]. The PF is population-based: at each instant of time the target state is represented by a set of particles, the particle cloud, that will move according to a state transition model, describing target motion. Examples of such target models are the constant velocity straight line trajectory and the horizontal turn. The set of particles can be drawn from any probability density function, thereby relaxing the Gaussian state vector and noise condition. The state transition model need not be linear, which makes the PF more generally applicable than the KF. As the observation from the sensor comes in, the processing will update the state vector for each individual particle. The target state vector and state error estimate are based on the ensemble-averaged statistics of the particle cloud. Like the KF, the PF is an iterative algorithm, that will yield state estimate updates at each new measurement.

The simulation in this work uses a 2-dimensional *x, y* orthogonal coordinate system. There are two sensors, S^1 and S^2, co-located at the origin on a single, non-moving platform. The data will be processed in the discrete time domain $t_k = kT$, where $T = 1$ s is the time interval between data points.

The target state vector $\mathbf{x} = \begin{bmatrix} x & \dot{x} & y & \dot{y} \end{bmatrix}^T$, where x and y are the target position and $\dot{x}$ and $\dot{y}$ are the target speed components (^{T} indicates the transpose). Measurement data are in polar coordinates (range r, Doppler $\dot{r}$ and bearing ϕ). Target motion is represented by a state-space process model. The process equation is given by

$$\mathbf{x}_k = \mathbf{F}\mathbf{x}_{k-1} + \mathbf{G}\mathbf{u}_{k-1} + \mathbf{v}_{k-1}, \tag{1}$$

where **F** is the state transition matrix, **G** is the input transmission matrix, **u** is the (optional) control input vector and **v** is the additive process noise, a zero-mean Gaussian process with covariance matrix $\mathbf{Q} = \mathbf{G}\mathbf{G}^T$ (probability distribution $p(\mathbf{v}) \sim N(0, \mathbf{Q})$). The matrix **F** relates the target state at the previous time step $\mathbf{x}_{k-1}$ to the current state $\mathbf{x}_k$. Here, target motion is described with a constant velocity process model. The matrix **G** relates the control input (e.g., evading manoeuvres in case of manned aircraft) to the target state.

The measurement model equation for both sensors is given by

$$\mathbf{z}_k^j = \mathbf{h}^j(\mathbf{x}_k) + \mathbf{w}_k^j, \tag{2}$$

where $\mathbf{z}^j$ is the measurement vector for sensor j ($j = 1$ or 2), $\mathbf{h}^j$ is the observer function and $\mathbf{w}^j$ is the measurement noise, a prior known, zero-mean Gaussian process with covariance matrix $\mathbf{R}^j$ (with probability distribution $p(\mathbf{v}) \sim N(0, \mathbf{R}^j)$). In this equation $\mathbf{h}^j$ relates the target state $\mathbf{x}_k$ to measurement $\mathbf{z}_k^j$. Furthermore, the probability of detection $0 \le p_d^j \le 1$.

In this work two different sensors will be defined. Sensor S^1 yields range (r), Doppler ($\dot{r}$) and bearing (ϕ) information

$$\mathbf{z}_k^1 = \begin{bmatrix} r_k \\ \dot{r}_k \\ \phi_k \end{bmatrix}, \ \mathbf{h}^1(\mathbf{x}_k) = \begin{bmatrix} \sqrt{x_k^2 + y_k^2} \\ \dfrac{x_k \dot{x}_k + y_k \dot{y}_k}{\sqrt{x_k^2 + y_k^2}} \\ \arctan \dfrac{y_k}{x_k} \end{bmatrix}, \ \mathbf{R}^1 = \mathrm{diag}\left(\begin{bmatrix} \sigma_r^2 & \sigma_{\dot{r}}^2 & \sigma_\phi^2 \end{bmatrix}\right), \tag{3}$$

whereas S^2 provides range and bearing only

$$\mathbf{z}_k^2 = \begin{bmatrix} r_k \\ \phi_k \end{bmatrix}, \ \mathbf{h}^2(\mathbf{x}_k) = \begin{bmatrix} \sqrt{x_k^2 + y_k^2} \\ \arctan \dfrac{y_k}{x_k} \end{bmatrix}, \ \mathbf{R}^2 = \mathrm{diag}\left(\begin{bmatrix} \sigma_r^2 & \sigma_\phi^2 \end{bmatrix}\right). \tag{4}$$

Note that the sensors have different Jacobian matrices $\mathbf{H}^j$ [Bar-Shalom et al., 2001], that may be considered as a sensitivity measure. They contain a set of gradients that indicate how a measurement component will change with a variation of a state vector component, and these will be a deciding factor in the sensor selection.

The PF state estimator consists of a sequence of processing steps: particle cloud initialisation, particle cloud propagation (the prediction step) and measurement update (weighted update after the measurement). Updating the particle cloud requires a resampling process and this step is skipped in case of a missing detection ($p_d < 1$).

In Fig. 1 the predicted and resampled particle clouds are depicted for $t = 1$, 15, 33 and 55 s. Observe the large-sized initial particle cloud at $t = 1$ s in the lower right corner. The wide predicted particle clouds become narrower after a measurement update and resampling. Since the sensors are positioned at the origin, one could infer some knowledge from the shape of the particle cloud about the measurement accuracies of the sensors. E.g., for $t =$ 15 and 55 s a sensor with a good range accuracy, but poor bearing accuracy yields the measurements.

Target state ($\hat{\mathbf{x}}_k$) and accuracy ($\hat{\mathbf{P}}_k$) are calculated with the first and second statistical moment (i.e., mean and covariance, respectively) of the particle cloud.

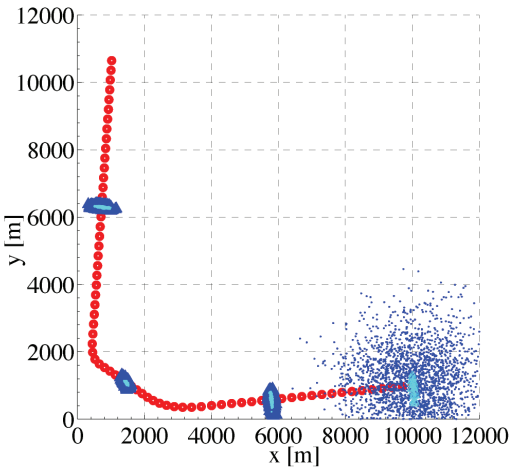

Figure 1. Predicted and resampled particle clouds of a particle filter state estimator. The red dotted line indicates a true target trajectory with states every 1 s. Note that the wide predicted particle clouds (blue dots) become narrower resampled particle clouds (cyan dots) after a measurement update. The clouds are plotted for t = 1, 15, 33 and 55 s with t = 1 s in the lower right corner. See Fig. 3 for more information about the target trajectory.

Sensor selection

The sensor selection algorithm (SSA) in [Ramdaras and Absil, 2006] is based on the Modified Riccati Equation (MRE) given by

$$\hat{\mathbf{P}}^j_{k+1|k} = \mathbf{F}\hat{\mathbf{P}}_{k|k-1}\mathbf{F}^T - p^j_d\mathbf{F}\hat{\mathbf{P}}_{k|k-1}\mathbf{H}^{j^T}\left(\mathbf{H}^j\hat{\mathbf{P}}_{k|k-1}\mathbf{H}^{j^T} + \mathbf{R}^j\right)^{-1}\mathbf{H}^j\hat{\mathbf{P}}_{k|k-1}\mathbf{F}^T + \mathbf{Q}, \tag{5}$$

where $\hat{\mathbf{P}}^j_{k+1|k}$ is the expected performance at time step $k+1$ for sensor j, $\hat{\mathbf{P}}_{k|k-1}$ is the predicted state error covariance matrix (that can be computed using the covariance of the particle cloud after the PF prediction step), p^j_d is the probability of detection and $\mathbf{H}^j$ is the Jacobian of the measurement matrix using the state estimate for the linearization process. One may observe that in (5) the sensor properties are included in p^j_d and the measurement accuracy $\mathbf{R}^j$. Also, for every sensor the instantaneous target state, and therefore the current geometry is represented in this equation by $\mathbf{H}^j$.

Criteria for sensor selection are based on considering specific elements from $\hat{\mathbf{P}}^j_{k+1|k}$ and minimising a cost function C^j. In [Ramdaras and Absil, 2006] the sensor selection criterion is the best expected target position accuracy (i.e., minimum positional variance in x and y, as expressed by σ^2_{xx}, σ^2_{xy} and σ^2_{yy} and therefore the cost function is defined as

$$C^j = \det\begin{pmatrix}\hat{\mathbf{P}}^j_{k+1|k}(1,1) & \hat{\mathbf{P}}^j_{k+1|k}(1,3)\\ \hat{\mathbf{P}}^j_{k+1|k}(3,1) & \hat{\mathbf{P}}^j_{k+1|k}(3,3)\end{pmatrix} = \det\begin{pmatrix}\hat{\sigma}^2_{xx} & \hat{\sigma}^2_{xy}\\ \hat{\sigma}^2_{xy} & \hat{\sigma}^2_{yy}\end{pmatrix}. \tag{6}$$

In [Ramdaras and Absil, 2007b] four alternative selection criteria are considered: best expected heading, range, Doppler and bearing accuracy.

In that case the cost function is expressed as [Zwaga and Driessen, 2005]

$$C^j = E[\mathbf{H}^c(\hat{\mathbf{x}}_{k|k-1})\hat{\mathbf{P}}^j_{k+1|k}\mathbf{H}^c(\hat{\mathbf{x}}_{k|k-1})^T], \tag{7}$$

where $\hat{\mathbf{x}}_{k|k-1}$ is the predicted target state vector and $\mathbf{H}^c$ is one of the following cases:

$$\mathbf{H}^c = \begin{cases} \left[\begin{array}{cccc} 0 & -\dfrac{\dot{y}}{\dot{x}^2+\dot{y}^2} & 0 & \dfrac{\dot{x}}{\dot{x}^2+\dot{y}^2}\end{array}\right] & \text{for heading,} \\ \left[\begin{array}{cccc} \dfrac{x}{r} & 0 & \dfrac{y}{r} & 0\end{array}\right] & \text{for range,} \\ \left[\begin{array}{cccc} \dfrac{\dot{x}}{r}-\dfrac{x^2\dot{x}+xy\dot{y}}{r^3} & \dfrac{x}{r} & \dfrac{\dot{y}}{r}-\dfrac{xy\dot{x}+y^2\dot{y}}{r^3} & \dfrac{y}{r}\end{array}\right] & \text{for Doppler,} \\ \left[\begin{array}{cccc} -\dfrac{y}{r^2} & 0 & \dfrac{x}{r^2} & 0\end{array}\right] & \text{for bearing/azimuth.} \end{cases} \tag{8}$$

Here, $r = \sqrt{x^2+y^2}$ and for convenience $\hat{\mathbf{x}}_{k|k-1} = [x_{k|k-1} \;\; \dot{x}_{k|k-1} \;\; y_{k|k-1} \;\; \dot{y}_{k|k-1}]^T$ is written as $\hat{\mathbf{x}}_{k|k-1} = [x \;\; \dot{x} \;\; y \;\; \dot{y}]^T$. For quantities that are directly measured, such as range, Doppler and bearing, $\mathbf{H}^c$ will contain the corresponding row from $\mathbf{H}^j$.

The optimal sensor $\hat{j}_k$ at time step k is selected by minimising the cost function as

$$\hat{j}_k = \arg\min\{C^j\}, j = 1,2,\ldots, j_{\max}. \tag{9}$$

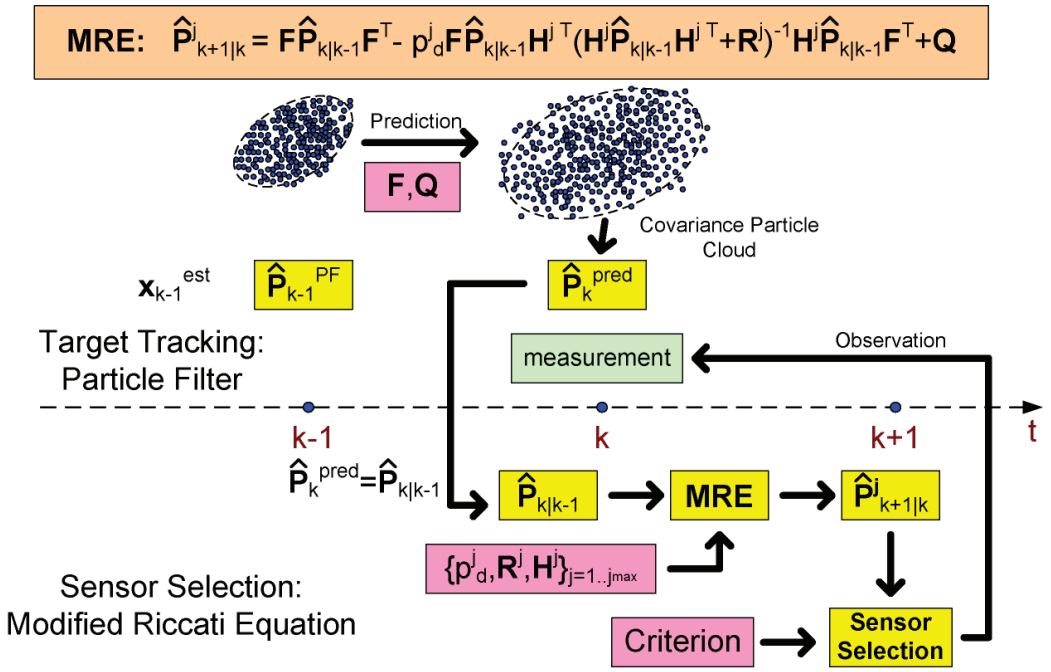

Figure 2. A schematic representation of the MRE SSA. The upper half of the figure represents the target tracking algorithm, while the lower part depicts the SSA (see explanation in the text).

In Fig. 2 the MRE SSA is shown in diagram. The upper half of the figure represents the target tracking algorithm, while the lower part depicts the SSA. The particle cloud at time step $k-1$ (see upper left) is progressed in the PF prediction step into a somewhat wider cloud at the current time step (see upper right). From this cloud $\hat{\mathbf{P}}_{k|k-1}$ is computed and used as input for the MRE equation together with the sensor properties (see upper red input block in the lower half of the figure). This yields an expected performance for each sensor. Based on the selection criterion (8) a sensor is selected to perform the measurement at time step k (measurement update step PF).

Simulation parameters

The computer simulation is based on a planar geometry with an area of 12×12 km^2 and a low-flying air target. The target trajectory consists of a closing and opening leg at zero altitude and constant flight speed of 300 m/s and two lateral manoeuvres (see Fig. 3): a 3g horizontal turn between $t = 22 - 28$ s and a 9g horizontal turn between $t = 38 - 40$ s. Two sensors are positioned on a non-moving platform at the origin. They represent two radar systems with a different measurement accuracy

$$\mathbf{R}^1 = \mathrm{diag}\left(\begin{bmatrix} 600 & 100 & 2.47\times 10^{-4} \end{bmatrix}\right),\ \mathbf{R}^2 = \mathrm{diag}\left(\begin{bmatrix} 1000 & 2.47\times 10^{-6} \end{bmatrix}\right).$$

Sensor S^1 yields good range and Doppler measurements ($\sigma_r = 24$ m and $\sigma_{\dot{r}} = 10$ m/s), while the bearing accuracy is poor ($\sigma_\phi = 0.9°$). Sensor S^2 yields no Doppler measurements (two elements in the matrix only), poor range information and high bearing accuracy ($\sigma_r = 32$ m and $\sigma_\phi = 0.09°$).

For the prior assumed probability of detection three cases are considered:

- Case 1: $p_d^{1,2} = 1$ (no missed detections),
- Case 2: $p_d^1 = 0.90$, $p_d^2 = 0.85$ (S^1 better than S^2) and
- Case 3: $p_d^1 = 0.85$, $p_d^2 = 0.90$ (situation reversed).

State estimation for target tracking is done with the PF. The particle cloud contains $N = 2500$ particles and for the resampling process Kitagawa's deterministic resampling algorithm [Doucet et al., 2001] has been used to get rid of the outliers relative to the observation. The PF update and resampling steps are skipped in case of a missing observation for a sensor with $p_d < 1$.

The performance of the sensor selection schemes is determined with simulated data over 70 s ($k_{\max} = 70$). The MRE SSA is based on one of the five sensor selection criteria: best expected position, heading, range, Doppler and bearing accuracy. In the case of fixed sensor selection (FSS) either S^1 (FSS-S1) or S^2 (FSS-S2) will be used along the entire target trajectory, in the case of random sensor selection (RSS) an uniformly distributed random variable will decide on which of the two equally probable sensors will do the next observation. The TRACE SSA is based on the minimum *trace* of the updated predicted error covariance as presented in [Chhetri et al., 2003].

The analysis includes the number of lost tracks, the quality of the state estimate and the sensor selection strategy. The results are ensemble-averaged over 1000 runs. Besides, the sensor selection strategy is evaluated for a planning horizon of $M = 1$ and $M = 6$ time steps ahead (for MRE SSA).

Simulation results

In the first part of this section MRE SSA is compared with RSS and FSS for $p_d^{1,2} = 1$. In the second part the MRE SSA is compared with the TRACE MRE for $p_d^{1,2} = 1$ and the third part describes two cases with $p_d < 1$ to demonstrate the benefits of the MRE SSA.

Comparison between MRE SSA, RSS and FSS for $p_d^{1,2} = 1$
The true target track and estimated target state are given in Fig. 3 for the three selection schemes and Case 1. Here state estimation with the MRE SSA is based on the best expected heading performance and is evaluated for a planning horizon of $M = 1$ and $M = 6$, while estimation with RSS and FSS implies $M = 1$. Besides, for FSS two options are considered: FSS-S1 (S^1 only) and FSS-S2 (S^2 only). Given the values of the measurement accuracies and due to the careful tuning of the PF there were no lost tracks.

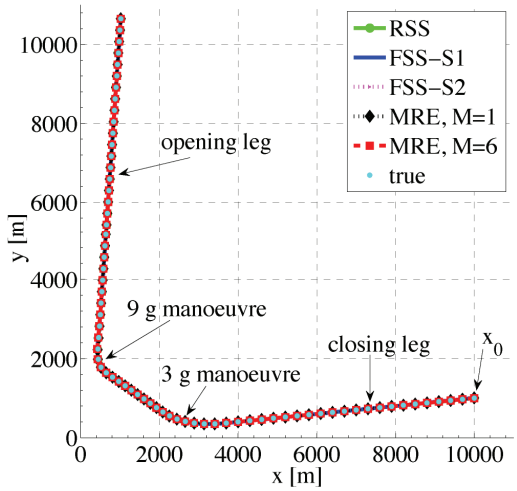

Figure 3. The true and estimated target state (average over 1000 runs). Sensor selection with the MRE SSA is based on the heading criterion. The planning horizons are $M = 1$ and $M = 6$; $p_d^{1,2} = 1$.

In the upper and middle plot of Fig. 4 the sensor selection strategy for Case 1 (MRE SSA based on the heading criterion), expressed as the number of times a sensor was selected, is depicted for a planning horizon of $M = 1$ and $M = 6$, respectively. S^2 is selected in the majority of cases. There is a clear change in sensor priority during the central part of the track, where S^1 with the additional Doppler information becomes more important. For $M = 6$ the change in sensor selection preference occurs after time instant $t = nM + 1$; note the changes after $t = 31$ s ($n = 5$) and $t = 43$ s ($n = 7$) in the middle plot. The lower plot shows the sensor selection strategy in case of random selection, and confirms the equal likelihood for both sensors. The trivial case of either FSS-S1 or FSS-S2 throughout is not plotted.

Whereas sensor selection based on best expected heading performance demonstrates sensor switching during the central part of the track, three alternative MRE sensor

selection criteria (best expected range, Doppler or bearing performance) show a different pattern. With these criteria and $p_d^{1,2} = 1$ there is no switching: the radar with the most accurate (i.e., the smallest) appropriate measurement error covariance term in $\mathbf{R}^{1,2}$ will be selected throughout the entire trajectory for both planning horizons $M = 1$ and $M = 6$ (not shown here). E.g., sensor selection with the range criterion gives preference to S^1, because $\sigma_{r_1}^2 < \sigma_{r_2}^2$.

In Fig. 5 the difference between the true and estimated target heading is given for the different selection schemes for Case 1: note the grouping of the MRE results with either FSS-S2 or FSS-S1. Sensor selection based on MRE SSA with the best expected heading accuracy criterion for $M = 1$ gives better results than RSS and FSS. Comparing MRE SSA for $M = 1$ with MRE SSA for $M = 6$ we may observe a difference in heading accuracy between $t = 3 - 8$ s, $t = 28 - 32$ s and $t = 42 - 45$ s. This corresponds to the difference in sensor selection strategies (see the upper and middle plot of Fig. 4). During the closing and opening leg FSS-S2 performs comparable to MRE SSA, during the central section there is agreement with FSS-S1. The RSS level lies between the lowest and highest target heading accuracy level. Note the humps in all curves between $t = 22 - 28$ s and $t = 38 - 42$ s due to the two lateral manoeuvres. The figure confirms that the actual performance is in agreement with the expected performance; it has been verified for the other selection criteria (not shown here).

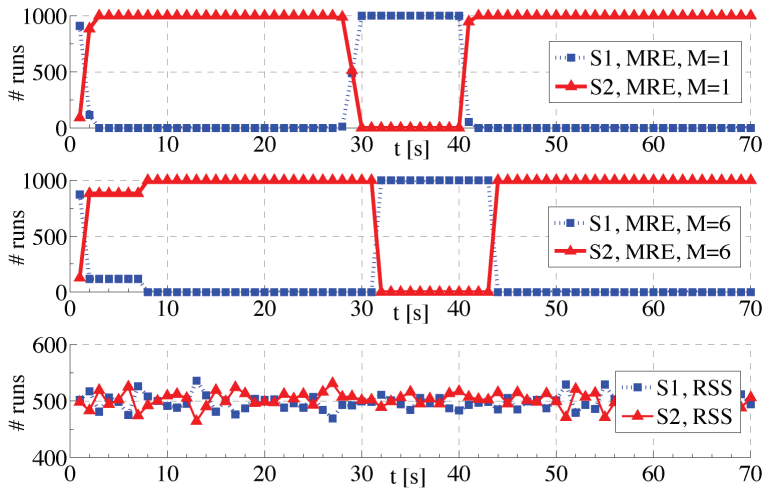

Figure 4. The sensor selection strategies with the MRE SSA based on the best expected heading accuracy (upper and middle plot) and with the RSS scheme (lower plot); $p_d^{1,2} = 1$. Note the dominance of sensor 2 in the closing and opening leg for MRE SSA; random selection is confirmed in the lower plot.

Comparison between MRE SSA and TRACE SSA for $p_d^{1,2} = 1$

Using the *trace* of the error covariance matrix for sensor selection as given in [Chhetri et al., 2003] implies an addition of dissimilar quantities (positions and speed) and available information in the error covariance matrix is not fully used. The comparison is done for Case 1 only (no missed detections) and the TRACE SSA was slightly modified: the *trace* of only the position elements in the predicted error covariance matrix is used, see (6).

In the upper plot of Fig. 6 the sensor selection strategy for the TRACE SSA is presented for Case 1 and $M = 1$, while the middle plot shows the selection strategy for the MRE SSA with the best expected position accuracy criterion. Observe that the MRE algorithm always

starts with sensor S^2 for $M = 1$, while the other algorithm always starts with S^1. For the closing and opening leg the sensor selection strategies are comparable, choosing sensor S^2 for the majority of cases; there the combination of highly accurate bearing plus somewhat poorer range accuracy yields the best position estimate. For the MRE SSA the additional Doppler information becomes more important during the central track section, as shown by the increase in S^1 use between $t = 30 - 50$ s. For the TRACE SSA the period of switching is longer ($t = 20 - 60$ s) and there is not a distinct preference for either S^1 or S^2. Between $t = 23 - 52$ s the selection strategy is comparable to the RSS strategy. The lower plot shows the selection strategy for the MRE SSA with $M = 6$ and the best expected position accuracy as criterion. One may notice the impact of extending the planning horizon from $M = 1$ to $M = 6$ during the central track section ($t = 30 - 50$ s): the preference for S^1 becomes more outspoken.

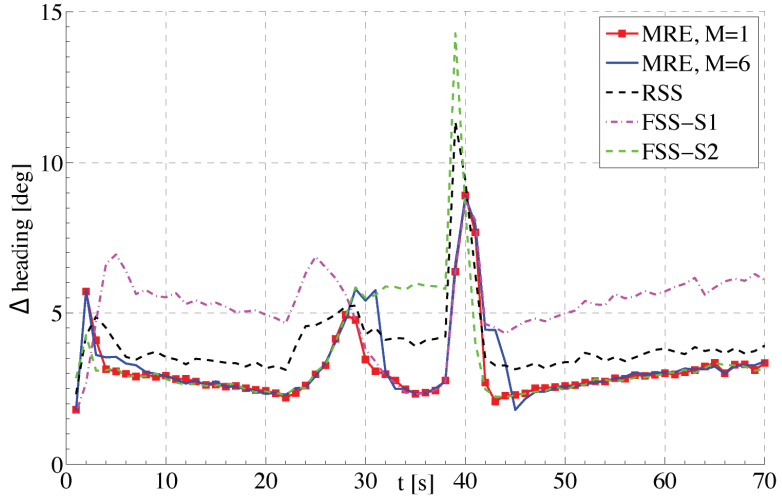

Figure 5. The difference between true and estimated target heading for three sensor selection schemes. For MRE SSA the planning horizons are $M = 1$ and $M = 6$; $p_d^{1,2} = 1$. Note how the performance of MRE SSA approaches that of a fixed sensor in different sections of the trajectory.

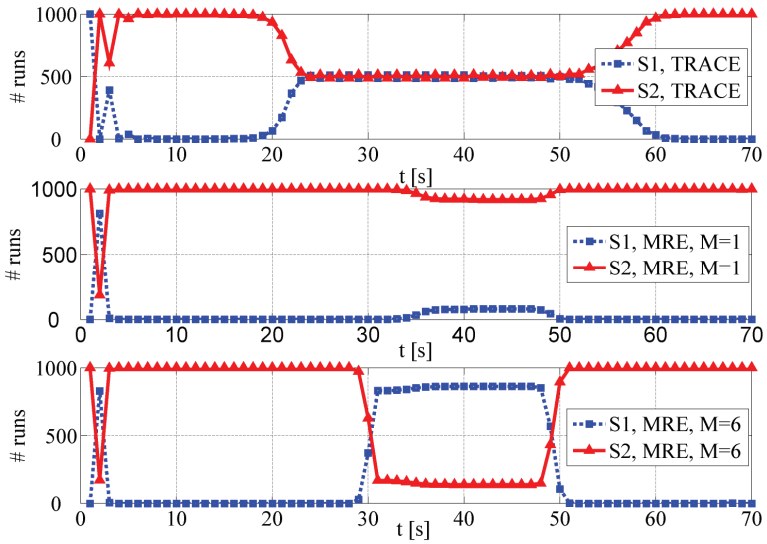

Figure 6. The sensor selection strategy of the TRACE SSA for a planning horizon of $M = 1$ (upper plot) and the MME SSA based on the best expected position accuracy, $M = 1$ and $M = 6$ (middle and lower plot); $p_d^{1,2} = 1$. During the closing and opening legs the sensor selection is comparable, while during the central section TRACE SSA is random.

Case 2 and 3 (lowering the detection probability)
In Figs. 7–11 the combination of selection criteria and p_d cases is deliberately chosen to test the flexibility and performance of the MRE SSA in a situation where either S^1 or S^2 currently yields the best accuracy.

The selection strategies for Case 1 (Fig. 4) and Case 2 for the opening and closing legs are comparable when the best expected heading criterion is used. Sensor 2 is selected in the majority of cases (see Fig. 7). There is a clear change in priority of sensors during the central part of the track, where S^1 with the additional Doppler information becomes more important. In Fig. 7 the sensor selection strategies for Case 2 are depicted for a planning horizon of $M = 1$ and $M = 6$. The lower plot shows the number of observations as a function of time. This is a check on the actual p_d during the simulations; note the central hump, due to the preference for S^1 with corresponding higher p_d.

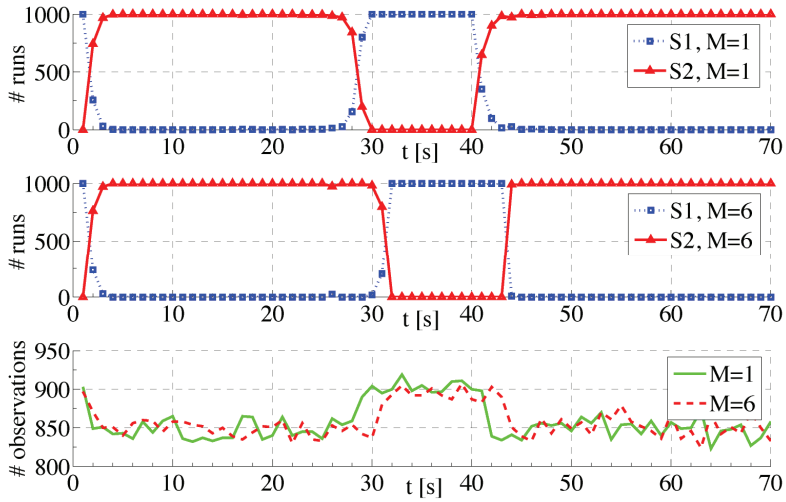

Figure 7. The sensor selection strategy based on the best expected heading accuracy (upper and middle plot) and the number of detections (lower plot) as a function of time, $P_d^1 = 0.90$ and $P_d^2 = 0.85$.

In Fig. 8 the sensor selection strategy of the MRE SSA with again the best expected heading criterion is depicted for Case 3 to compare the reversed situation of the p_d for the same planning horizon. Observe the complete dominance of S^2 during the entire track. The earlier preference for S^1 at $t = 1$ s and in the central part ($t = 30 - 40$ s) has completely disappeared. Obviously the effect of the swapped p_d-values outweighs the additional information obtained with S^1 during the target turns. The actual number of observations (lower plot) confirms $p_d^2 = 0.90$.

In Fig. 9 the selection strategy for Case 3 is presented for MRE SSA with the best expected range accuracy as selection criterion and RSS (upper and middle plot). The planning horizon is $M = 1$. Observe in the upper plot the complete preference for S^1 during the entire track except for $t = 1 - 2$ s. For $t = 3 - 70$ s the selection strategy is the same as FSS-S1. Although $p_d^1 < p_d^2$, the better range accuracy achievable with S^1 dominates the sensor selection strategy. In the lower plot the actual p_d's once again confirm the a priori assumed values during the simulations. Note the change from $p_d = 0.90$ to $p_d = 0.85$ for the MRE selection scheme during $t = 1 - 2$ s. This corresponds with the selection strategy during this part of the track. For RSS the average $p_d \approx 0.875$.

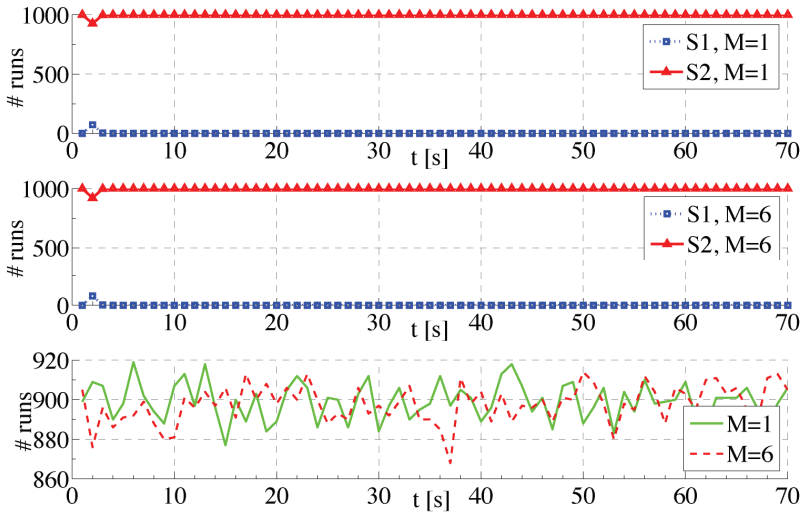

Figure 8. The sensor selection strategy based on the best expected heading accuracy (upper and middle plot) and the number of detections (lower plot) as a function of time, $P_d^1 = 0.85$ and $P_d^2 = 0.90$.

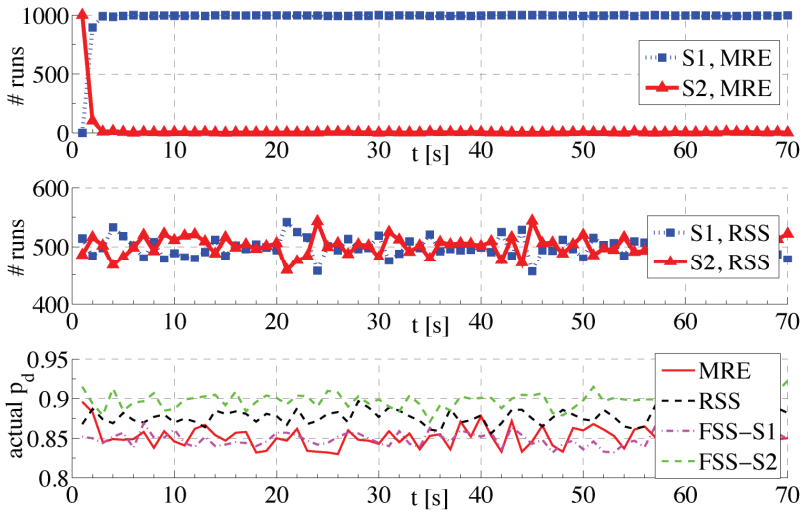

Figure 9. The sensor selection strategies with the MRE SSA (range criterion, $M = 1$) and the RSS scheme (upper and middle plot), and the actual P_d's (lower plot); $P_d^1 = 0.85$ and $P_d^2 = 0.90$.

In Fig. 10 the difference between the true and estimated target range is given for the MRE SSA based on five sensor selection criteria for Case 3 and $M = 1$: best expected position, heading, range, Doppler and bearing accuracy. As expected, sensor selection based on the MRE SSA with the range criterion performs better than the other selection criteria. There is one exception: MRE SSA with the Doppler criterion performs better during $t = 1 - 10$ s due to two effects: for $t = 1 - 2$ s the selection strategy based on the Doppler criterion has a solid preference for S^1, which is comparable to FSS-S1 (not shown here), while for $t = 3 - 10$ s (and the other parts where the Doppler line is below the range line) statistical effects become clear, since the process noise ($\mathbf{v}_k^j$) and the measurement noise $\mathbf{w}_k^j$ are simulated every run instead of using a fixed data set during all runs and for all criteria. As expected from the values of the elements in $\mathbf{R}^1$ and $\mathbf{R}^2$, S^1 indeed yields better range accuracy.

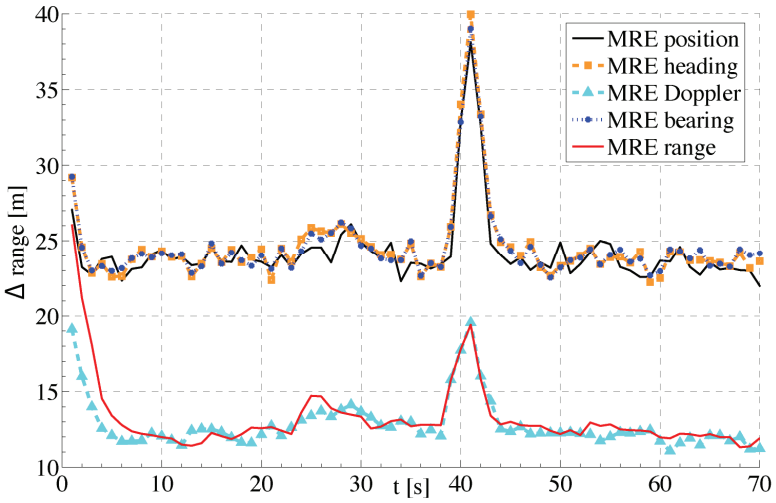

Figure 10. The difference between true and estimated target range for five sensor selection criteria with the MRE SSA. The planning horizon $M = 1$; $P_d^1 = 0.85$ and $P_d^2 = 0.90$.

In Fig. 11 the difference between the true and estimated target range is given for the three sensor selection schemes for Case 3. Observe that sensor selection based on the MRE SSA with the best expected range accuracy as selection criterion performs better than RSS and FSS-S2. FSS-S1 performs better during $t = 1 - 10$ s due to the difference in sensor selection strategy in the beginning of the track.

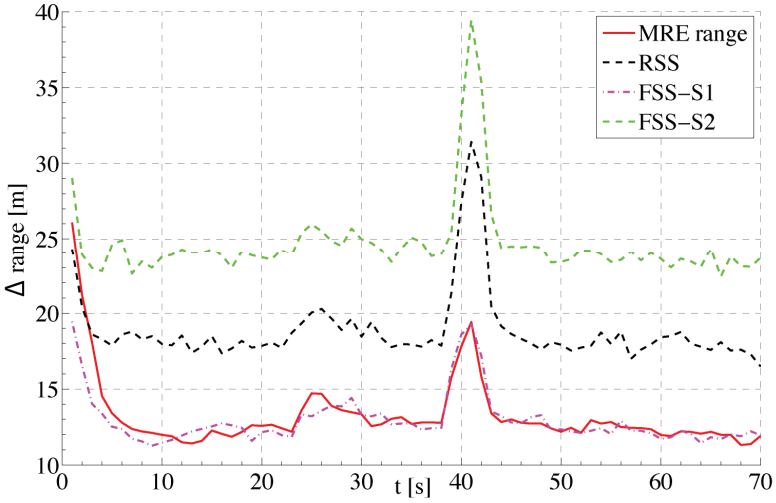

Figure 11. The difference between true and estimated target range for three sensor selection schemes. The planning horizon $M = 1$; $P_d^1 = 0.85$ and $P_d^2 = 0.90$.

The results of these two cases demonstrate the benefits and general applicability of the MRE SSA for a fairly realistic target scenario and sensor properties, such as the measurement accuracy and the probability of detection.

Conclusions, future research topics and implementation aspects

In current NLDA research on air and surface picture compilation with a network of naval radar systems a *sensor selection* approach is based on the Particle Filter target tracking technique and a minimisation approach to the cost function, derived from the Modified Riccati Equation (MRE).

In order to evaluate the benefits of the MRE sensor selection algorithm (SSA) this paper compares four different sensor selection schemes in a target tracking scenario: MRE SSA, random sensor selection (RSS), fixed sensor selection (FSS) and sensor selection based on the *trace* of the updated predicted error covariance matrix (TRACE SSA).

Several expected performance criteria were used for the MRE SSA that should yield maximum accuracy for specific target state parameters (best expected position, heading, range, Doppler and bearing accuracy). Several planning horizons (1 and 6 time steps ahead) were compared and the effect of reduced detection probability (p_d between 0.85 and 1.0) was studied. Results of the computer simulations include the sensor selection strategy (pick one from a set of two radars to do the observation) and the performance analysis (the quality of the state estimate during the target trajectory).

For the MRE SSA with the best expected range, Doppler or bearing performance as criterion, the sensor with the most accurate (i.e., the smallest) appropriate measurement error covariance term will be selected throughout the entire trajectory for both $M = 1$ and $M = 6$ planning horizons. The actual performance, expressed by the difference between the true and estimated state, is in agreement with the expected performance. These simulations serve to verify the applicability of this sensor selection algorithm for fairly realistic sensor properties and an air target scenario.

Sensor selection based on the MRE performs better than RSS. For the best expected range or Doppler performance the sensor selection strategy of the MRE SSA is comparable with FSS-S1, for the best expected bearing performance it is comparable with FSS-S2. These latter two cases were deliberately chosen to demonstrate the flexibility and quality of the MRE SSA in situations where a single sensor currently yields the best performance. For the best expected heading and position performance the MRE SSA gives better results than FSS. For the best expected position performance the MRE SSA gives better results than TRACE SSA.

For the values of p_d considered, there were no lost tracks and the quality of the state estimate is good. Although the ratio of the corresponding elements in the radar measurement error covariance matrices $\mathbf{R}^1$ and $\mathbf{R}^2$ dominates the sensor selection strategy for $p_d^{1,2} = 1$, the effect of the prior known values of p_d in the MRE is noticeable when the difference between p_d^1 and p_d^2 increases. For the MRE SSA an increase of the planning horizon from $M = 1$ to $M = 6$ has no significant deteriorating effect on track accuracy level.

Until now the research has focused on a thorough investigation of the various forms of the sensor selection algorithm. Extending the analysis to more realistic cases is straightforward for some aspects:

- Inclusion of the third spatial dimension, i.e., altitude, only means an additional term in the state and observation vectors. The selection algorithm is identical for a 3-D geometry and hardly needs software modification.
- Autonomously moving platforms can be incorporated in the selection scheme,

since the observations include relative kinematic quantities (currently both sensors are positioned at the origin).

- Multiple targets can be handled by applying the selection algorithm sequentially to each target. For each individual target the best suitable sensor will be determined over a certain planning horizon, and the selection strategy is based on target-related accuracy criteria. When simultaneous sensor claims arise from multiple targets, this has to be handled at a higher level of the sensor management architecture, where threat prioritisation and sensor scheduling take place.
- The way ahead for this work is to study the sensor localisation topic, i.e., moving the platforms around in such a way that future observations will again yield best expected accuracy for specific target state attributes, while maintaining adequate sensor coverage capability over a certain operational area. A number of localisation techniques will be implemented and tested in a computer simulation for realistic scenarios.

Next, a software architecture has to be defined, that somehow merges the sensor selection and localisation approaches. This requires definition of a certain sensor management hierarchy (localisation gets higher priority than selection, or the other way round). Another aspect of interest is the relevance of reliable communication links between the moving operational units. Research questions are: what happens if there is temporary loss of communications (no longer in line-of-sight, which is relevant in a wider area scenario where ships lie over the horizon and there is neither an aircraft nor a satellite relay station option)? How robust is the network sensor management approach? Can there be a fallback to the local optimisation process, with picture compilation at the single unit level? How is this temporary single ship approach later merged into a restarted global sensor grid optimisation?

At some point the mix of both sensor platforms and targets will have to be extended. It will be most interesting to see how the network sensor management strategy behaves in a setting with a wide range of kinematic and dynamic parameters (just think of the different speeds and manoeuvring capabilities of air vs. surface units).

If this research leads to a network sensor management strategy, that has demonstrated its capability in ample computer simulations, a most challenging next step would be to test the approach at sea. Since in the research set-up data exchange between units takes place at the plot level (i.e., target state attributes, no raw sensor data), communication bandwidth between units should not be a problem. However, at longer ranges in a more realistic exercise scenario (e.g., 200 × 200 km^2) the communication relay function will have to be realised (by either helicopter, UAV or satellite). And obviously, organising a test at sea involving multiple surface and air units and targets will be a complex and costly operation, but an unavoidable step on the way to operational deployment. As distributed system concepts with a multitude of military systems are becoming a reality, the requirement for global network optimisation and sensor grid management is evident. This research hopes to make a contribution to that end.

Designing the software architecture to coordinate the sensor grid as part of a Network Centric Warfare and realise Network-Enabled Capabilities certainly is a challenging and new subject of rewarding scientific research at the NLDA.

Acknowledgements

The authors would like to thank L.P. Ligthart and P. van Genderen, both with the International Research Centre for Telecommunications and Radar of the Delft University of Technology, and J.N. Driessen from Thales Nederland B.V., for their contribution to the scientific discussion on this subject.

References

Alberts, D., Garstka, J. and Stein, F. (2000) *Network Centric Warfare: Developing and Leveraging Information Superiority*. CCPR Publication Series, 2nd edition.

Bar-Shalom, Y. and Fortmann, T. (1988) *Tracking and Data Association*. Academic Press, New York.

Bar-Shalom, Y., Li, X. and Kirubarajan, T. (2001) *Estimation with Applications to Tracking and Navigation: Theory, Algorithms and Software*. John Wiley & Sons, Inc.

Boers, Y. and Driessen, H. (2006a) On the Modified Riccati Equation and its Application to Target Tracking. *IEE Proceedings - Radar, Sonar and Navigation*.

Boers, Y. and Driessen, H. (2006b) Results on the Modified Riccati Equation: Target Tracking Applications. *IEEE Transactions on Aerospace and Electronic Systems*, 42(1):379–384.

Boyd, J. (1987-1992) A Discource on Winning and Losing. Unpublished briefing notes, available at: http://www.d-n-i.net/richards/boyds_ooda_loop.ppt.

Cebrowski, K. and Garstka, J. (1998) Network-Centric Warfare: Its Origin and Future. *Proceedings of the Naval Institute*, 124(1):28–35.

Chhetri, A., Morrell, D. and Papandreou-Suppappola, A. (2003) Scheduling Multiple Sensors Using Particle Filters in Target Tracking. *IEEE Proceedings of the Statistical and Signal Processing Workshop*.

Doucet, A., de Freitas, N. and Gordon, N. (2001) *Sequential Monte Carlo Methods in Practice: Statistics for Engineering and Information Science*. Springer-Verlag New York.

Gordon, N., Salmond, D. and Smith, A. (1993) A Novel Approach to Non-Linear/ Non-Gaussian Bayesian State Estimation. *IEE Proceedings-F.*, 140(2).

Johns Hopkins APL (1995) The Cooperative Engagement Capability. *Johns Hopkins APL Technical Digest*, 16(4):377–396.

Kalman, R. (1960) A New Approach to Linear Filtering and Prediction Problems. *Transactions of the ASME - Journal of Basic Engineering*, 82:35–45.

Molina López, J., Jiménez Rodríquez, F. and Casar Corredera, J. (1995). Fuzzy Reasoning for Multisensor Management. *Proceedings of the IEEE Conference on Systems, Man and Cybernetics: "Intelligent Systems for the 21st Century"*, 2:1398–1403.

Ramdaras, U. and Absil, F. (2006) Networks of Maritime Radar Systems: Sensor Selection Algorithm for $p_d < 1$ Based on the Modified Riccati Equation. *Proceedings of the IEEE Nonlinear Statistical Signal Processing Workshop: Classical, Unscented and Particle Filtering Methods*.

Ramdaras, U. and Absil, F. (2007a) Sensor Selection: the Modified Riccati Equation Approach Compared with other Selection Schemes. *Proceedings of the Tenth International Conference on Information Fusion*.

Ramdaras, U. and Absil, F. (2007b) Target Tracking in Sensor Networks: Criteria for Sensor Selection. *Proceedings of the IEEE Radar Conference*, pp 192–196.

Ristic, B., Arulampalam, S. and Gordon, N. (2004) *Beyond the Kalman Filter: Particle Filters for Tracking Applications.* Artech House, Inc.

Sijtsma, F. (1995) Cooperative Engagement Capability: Interessant voor de KM? *Marineblad*, 105(4):100–103 (in Dutch).

STATOR (2005) Sensor Tuning and Timing on Object Request (STATOR), Final Report. Technical Report KIM-IWW-2005-01, Royal Netherlands Naval College, International Research Centre for Telecommunications- transmission and Radar of the Delft University of Technology and Thales Naval Nederland.

Yilmazer, N. and Osadciw, L. (2004) Sensor Management and Bayesian Networks. *Proceedings of SPIE – Multisensor, Multisource Information Fusion: Architectures, Algorithms, and Applications*, 5434:238–248.

Zwaga, J. and Driessen, H. (2005) Tracking Performance Constrained MFR Parameter Control: Applying Constraints on Prediction Accuracy. *Proceedings of the Eighth International Conference on Information Fusion*, pp 546–551.